Research Article | Vol. 29, No. 25 / 6 Dec 2021 / Optics Express 41643
Optics EXPRESS

Metasurface-based coupling suppression for wideband multiple-input-multiple-output antenna arrays

XIAOJUN ZOU, GUANGMING WANG,* YAWEI WANG, AND BINFENG ZONG

Air and Missile Defense College, Air Force Engineering University, Xi'an 710051, Shaanxi, China
**wgming01@sina.com*

Abstract: Wideband decoupling requires simultaneous improvements in the performance of an antenna array in its operating band. In this paper, a metasurface structure is proposed to accomplish this difficult task in wideband dual-layer coupled patch multiple-input-multiple-output (MIMO) antenna arrays. The decoupling mechanism is analyzed based on network and field theories, and dual-band response is achieved by incorporating multilayer hybrid split-ring resonators to create a meta-atom equipped with single negative property. By introducing the metasurface into the H-plane coupled MIMO array, the working bandwidth improves from 21.7% to 25.4%, mutual coupling is suppressed to less than −20 dB, gains mostly improve, and radiation patterns are modified. Moreover, the metasurface-based decoupling structure is extended to the E-plane coupled and two-dimensional arrays, exhibiting the same decoupling capability in the 22.9% and 23.6% bandwidths, respectively. Compared with existing metasurface-based decoupling works, the proposed metasurface, which is designed to be coplanar with the array, brings about no change to the array profile and possesses a wider decoupling bandwidth. These results indicate its potential in efficiently decoupling multielement wideband MIMO antenna arrays.

1. Introduction

Ever since metasurface was proposed in 2011 [1], it has been exploited for various functions on account of its excellent capability of wavefront manipulation, including anomalous reflection [2], focusing [3], multiple beams [4], vortex generation [5], surface plasmon polariton excitation [6], and radar cross-section reduction [7]. Moreover, metasurfaces are widely employed to improve antenna performance; the most common ones are high-gain realization [8], bandwidth enhancement [9], dual-frequency/multi-frequency operation [10], and miniaturization [11]. Meanwhile, metasurface-based decoupling technology is applied to alleviate mutual coupling among array antenna elements—a significant problem in designing MIMO (multiple-input-multiple-output) antenna arrays.

Mutual coupling typically occurs when array elements are densely arranged, leading to a series of effects detrimental to antenna performance, especially for MIMO arrays. These effects include impedance mismatching, radiation pattern deviation, side-lobe level increase, scan blindness, high signal correlation, and low radiation spectral efficiency [12]. Although mutual coupling is generally disregarded when element spacing exceeds half of the wavelength, it cannot be ignored with the increasing demand for miniaturization and limited space. Accordingly, various decoupling methods have been devised to reduce mutual coupling among antenna array elements; among these, the use of a metasurface is increasingly proposed. Typically, single negative metamaterials [13–19] are widely applied to effectively reduce mutual coupling using specific permittivity and permeability properties. Bait-Suwailam first proposed the use of single negative magnetic metamaterials to decouple closely spaced high-profile monopole antenna elements [13].

#444293 https://doi.org/10.1364/OE.444293
Journal © 2021 Received 26 Sep 2021; revised 8 Nov 2021; accepted 15 Nov 2021; published 30 Nov 2021

Optics EXPRESS

To reduce coupling among H-plane coupled patch antennas, waveguided metamaterials exhibiting magnetic resonance materials and realized by crossed-meander-line slits were employed [15]. Meta-structures consisting of two types of resonators were vertically inserted between two dual-polarized wideband patch antennas to improve isolation by 7.15 dB [16]. Furthermore, single negative metamaterial was introduced for decoupling a circularly polarized conformal array antenna [18]. Because a metasurface is derived from a metamaterial, they have similar characteristics that can decouple MIMO arrays [20–25]. To implement decoupling, a suspended metasurface, which was equivalent to a negative permeability medium, was placed above the patch antenna array [20]. Luan proposed a simple metasurface superstrate consisting of periodic ring slots to suppress the mutual coupling between E-plane and H-plane patch antennas [21]. Liu adopted a metasurface superstrate composed of two non-uniform cut wires to decouple dual-band antennas [24]. Moreover, a bidirectional absorbing metasurface was embedded between two Yagi antennas to reduce mutual coupling to approximately 38 dB at the resonant frequency [26]. However, these metasurfaces, which were usually placed above antenna arrays, could enlarge the array profiles; a few of them were applied to wideband decoupling.

In this paper, a novel metasurface is proposed to decouple wideband MIMO antenna arrays, i.e., dual-layer coupled microstrip patch antenna arrays. First, the operating principle is derived from network and field theories and implemented using a multilayer hybrid split-ring resonator (SRR) meta-atom, which exhibits dual-band response and single negative property. Then, a 7×2 sequence formed by the modified meta-atom is employed in decoupling a two-element H-plane coupled array whose working bandwidth improves from 21.7% to 25.4%. By suppressing the mutual coupling to less than -20 dB, gains mostly improve, and radiation patterns are modified. The proposed metasurface is inserted into a three-element array to assess its decoupling effectiveness in multielement linear MIMO arrays. The metasurface successfully unlocks the array arrangement direction by decoupling the E-plane antenna array; the bandwidth is extended to 22.9%, and coupling is reduced to less than -20 dB. The metasurface is eventually loaded to a constructed two-dimensional MIMO antenna array to verify its decoupling capability in a multielement two-dimensional array; similar results are achieved. Compared with reports on metasurface-based decoupling, the proposed metasurface does not influence the array profile and has a wider decoupling bandwidth. Thus, it has the potential of efficiently decoupling multielement wideband MIMO antenna arrays.

2. Operating principle and meta-atom design

To efficiently alleviate mutual coupling between array elements, its cause and the operating principle of decoupling are initially analyzed. On one hand, assume a two-element MIMO antenna array arranged along the y-axis, which is depicted in Fig. 1(a); only port 1 is excited, whereas port 2 is terminated to a 50Ω load, then the mutual coupling occurs from the radiated electromagnetic field. The model can be equivalent to a two-port network illustrated in Fig. 1(c), and its relationship of input and output voltages is represented by S-parameters [13].

$$\begin{bmatrix} V_1^o \\ V_2^o \end{bmatrix} = \begin{bmatrix} S_{11} & S_{12} \\ S_{21} & S_{22} \end{bmatrix} \begin{bmatrix} V_1^i \\ V_2^i \end{bmatrix} \tag{1}$$

where V_1^i, V_2^i, V_1^o and V_2^o denote the input and output voltages of port 1 and port 2, respectively, and S_{12} and S_{21} represent the coupling coefficients. When the network is lossless, reciprocal and matched, Eq. (1) can be further simplified to

$$\begin{bmatrix} V_1^o \\ V_2^o \end{bmatrix} = \begin{bmatrix} 0 & S_{12} \\ S_{21} & 0 \end{bmatrix} \begin{bmatrix} V_1^i \\ V_2^i \end{bmatrix} \tag{2}$$

Optics EXPRESS

Therefore, it is obvious that when S_{12}=S_{21}=0, the mutual coupling can be removed, that is to say, the mutual impedances Z_{12} and Z_{21} should be purely reactive. It is known that the equivalent impedance of single negative meta-atom usually presents zero real part and large imaginary part [13,14], thus single negative metasurface is potential to be employed to reduce mutual coupling.

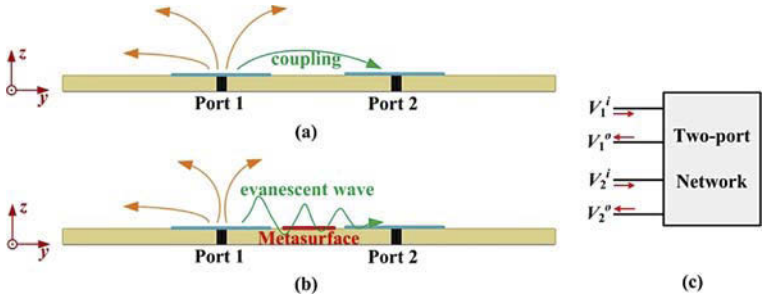

Fig. 1. Schematic of the operating principle. (a) Electric field distribution of a two-element MIMO coupled antenna array; (b) electric field distribution of a two-element MIMO antenna array loaded with decoupling metasurface; (c) the equivalent network model.

On the other hand, to better reveal the decoupling principle of single negative metasurface, its mechanism is analyzed from the field perspective. For the unexcited array element in Fig. 1(a), coupling results from the y-component of the electric field travelling along the y-axis. This can be expressed as

$$E(y,t) = E_0 e^{-jky} \cdot e^{jwt} \tag{3}$$

where k is the wavenumber related to the material. If the equivalent permittivity, ε_r, and permeability, μ_r, of the material are known, the wavenumber can be expressed as follows.

$$k = \omega \cdot \sqrt{\mu_r \mu_0 \cdot \varepsilon_r \varepsilon_0} = k_0 \cdot \sqrt{\mu_r \cdot \varepsilon_r} \tag{4}$$

Then, the electric field can be further represented by the following.

$$E(y,t) = E_0 e^{-jk_0 \cdot \sqrt{\mu_r \cdot \varepsilon_r} \cdot y} \cdot e^{jwt} \tag{5}$$

By applying single negative material to alleviate the mutual coupling between the array elements, either permittivity or permeability is negative, and the other is positive, i.e., ε_r<0 and μ_r>0 or ε_r>0 and μ_r<0. Then, the electric field can be eventually expressed as follows.

$$E(y,t) = E_0 e^{-jk_0 \cdot \sqrt{-|\mu_r| \cdot |\varepsilon_r|} \cdot y} \cdot e^{jwt} = E_0 e^{-jk_0 \cdot j\sqrt{|\mu_r| \cdot |\varepsilon_r|} \cdot y} \cdot e^{jwt} = E_0 e^{k_0 \cdot \sqrt{|\mu_r| \cdot |\varepsilon_r|} \cdot y} \cdot e^{jwt} \tag{6}$$

Apparently, the electromagnetic wave travelling along y-axis turns to be evanescent to enable the wave to travel mainly along the z-axis, which is demonstrated in Fig. 1(b), then the mutual coupling is reduced.

Accordingly, the objective is to propose a metasurface possessing single negative property. The proposed multilayer hybrid SRR meta-atom is shown in Fig. 2. To match the assumed traditional wideband antenna array element of a dual-layer coupled microstrip patch antenna, the meta-atom consists of two substrates, three SRRs, and ground plane. The modified upper and lower SRR elements formed by two traditional back-to-back SRRs are displayed in Fig. 2(b) and (c), respectively. Two uniform upper SRRs are printed on both sides of the upper substrate, whereas the relatively large SRR and ground plane are printed on the top and bottom sides of the lower substrate. The substrates, which are separated by an air gap (height: h_2), employ an FR4 composite material whose relative permittivity and loss tangent are 4.3 and 0.02, respectively. The detailed dimensions of the proposed meta-atom are listed in Table 1. Through simulation

Optics EXPRESS

in Ansys HFSS and setting the periodic boundary, the S-parameters of the multilayer hybrid SRR meta-atom are obtained, as plotted in Fig. 2(d). Then, the meta-atom's effective relative permittivity, ε_r, and permeability, μ_r, shown in Fig. 2(e), are derived according to the method presented in [27]. Apparently, the dual-band response is excited because of various SRRs. In these two bands, i.e., 4.64-4.76 and 5.16-5.76 GHz, the retrieved effective relative permittivity is positive, whereas the permeability is negative, indicating that the proposed meta-atom is single negative. Moreover, because the two bands are close to each other, the metasurface has potential for decoupling wideband antenna arrays. Also, to better optimize the meta-atom dimensions in the following antenna arrays, the single negative property with varying structure parameters is analyzed in Fig. 2(f) and (g) by choosing two main ones. It is apparent that with the increasement of the gap of the larger SRR, g_1, the cutoff frequency turns higher. While for the stretched part, c_2, of the smaller SRR, when c_2 is from 0.6 mm to 1.4 mm within the edge of the SRR, larger c_2 brings about narrower bandwidth due to the lower corresponding frequency. And when c_2 is out of the edge, the bandwidth is enlarged. Thus, the dimensions of the meta-atom can be tuned in the application of the antenna decoupling, as only the bandwidth and cutoff frequency vary, while the single negative property remains.

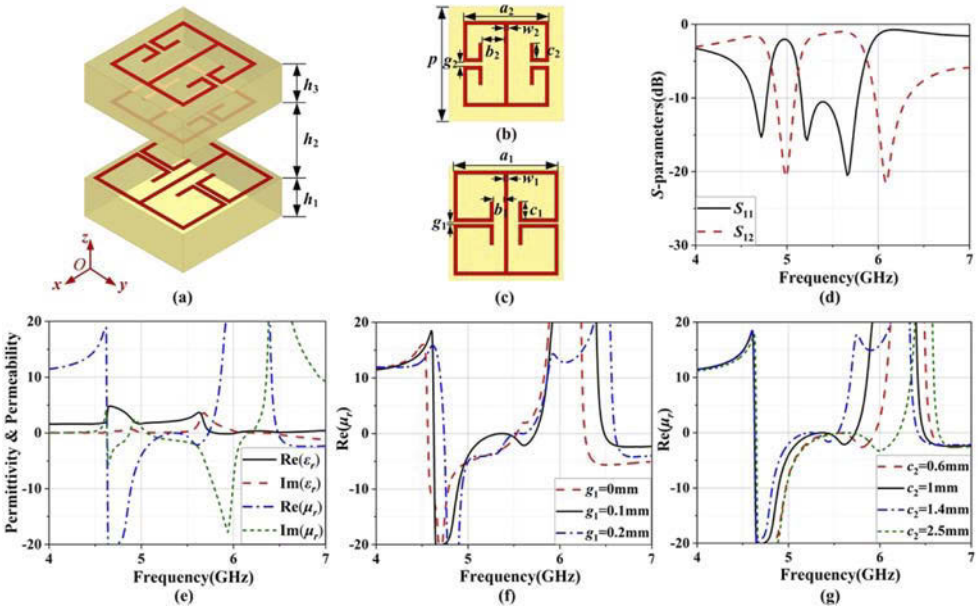

Fig. 2. Schematic and properties of proposed multilayer hybrid SRR meta-atom. (a) Overall structure; (b) upper SRR; (c) lower SRR; (d) S-parameters of meta-atom; (e) retrieved effective relative permittivity and permeability from S-parameters; (f) real part of the effective permeability with different g_1; (g) real part of the effective permeability with different c_2.

3. Decoupling of wideband MIMO antenna arrays

The selected dual-layer coupled microstrip patch antenna element is illustrated in Fig. 3. The antenna is composed of two uniform patches, two substrates and ground plane. The main and parasitic patches, which are equal in size ($w_p \times l_p$), are printed on the top layers of the lower and upper substrates, respectively; these substrates and metasurface share the same parameters. The main patch is fed by a coaxial probe, which is x_f-distance away from the short side. The dimensions of the patch antenna are listed in Table 1. Then the characteristics of the single

Optics EXPRESS

antenna are plotted in Fig. 3(d), which shows that the operating band is 4.36-5.48 GHz (22.8%) and the gain varies between 6.89 dBi and 7.82 dBi. And the aim of decoupling is to enable the performance of antenna element in an array to retain that of the single antenna as closely as possible.

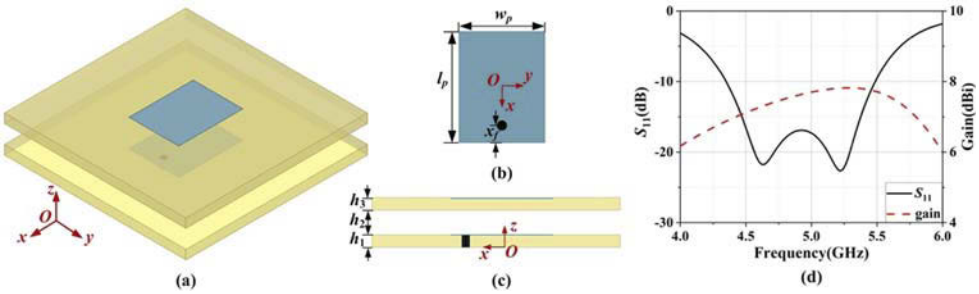

Fig. 3. Geometry and characteristics of dual-layer coupled microstrip patch antenna. (a) Overall structure; (b) main patch; (c) side view; (d) S_{11} and gain.

Table 1. Dimensions of meta-atom and patch antenna (unit: mm).

a_1	b_1	c_1	g_1	w_1	p
5.5	0.5	0.9	0.1	0.2	6
a_2	b_2	c_2	g_2	w_2	d
4.5	1.1	1	0.2	0.2	11
l_p	w_p	x_f	h_1	h_2	h_3
14.2	11	2.2	2	4	2

Initially, a two-element H-plane coupled MIMO antenna array is arranged with the proposed metasurface for decoupling, as shown in Fig. 4. The edge-to-edge distance of elements is $d = 11$ mm ($0.18\lambda_0$); consequently, the center-to-center distance is $0.37\lambda_0$ (where λ_0 is the wavelength at the 5 GHz center frequency). The metasurface, composed of 7 × 2 meta-atoms, is inserted between the array elements. The metasurface is observed to fit well in the antenna array. Moreover, different from most metasurface-based decoupling structures placed above the original antenna arrays, the proposed metasurface has no impact on the array profile, which is consistently $0.13\lambda_0$. To achieve better decoupling performance, the structure parameters of the meta-atom are primely adjusted.

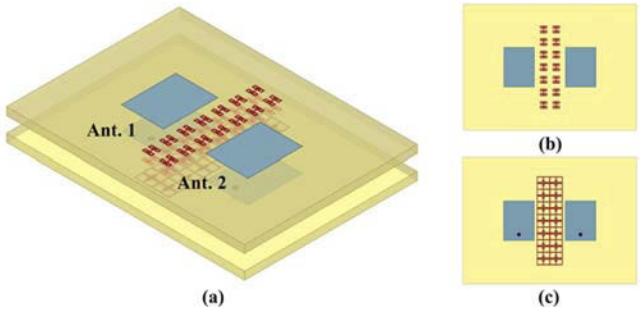

Fig. 4. Geometry of decoupled two-element H-plane coupled MIMO antenna array with metasurface. (a) Overall structure; (b) parasitic patches with upper SRRs; (c) main patches with lower SRRs.

Optics EXPRESS

To verify the decoupling capability of the proposed metasurface, both coupled and decoupled arrays with and without the metasurface are fabricated, assembled, and measured. The fabricated porotypes, comparison of simulated and measured *S*-parameters, and gains of antenna arrays are demonstrated in Fig. 5. Based on the reflection coefficients shown in Fig. 5(a), the simulated operating band of the antenna array widens from 4.44-5.52 GHz (21.7%) to 4.26-5.50 GHz (25.4%) by loading the metasurface; these results agree well with the measurements. It is obvious that in the presence of mutual coupling, the bandwidth of the coupled array is a little degraded compared with that of the single antenna, but is recovered and further extended after decoupling, which is mainly due to the introduction of new multiple resonances resulting from the coupling between the array and metasurface [22]. Before decoupling, mutual coupling among array elements is strong, especially at low band because of the relatively small electrical size. The maximum simulated and measured values occur at 4.5 GHz, reaching −12.0 and −9.6 dB, respectively. However, owing to the inserted metasurface, the coupling coefficient is suppressed to less than −20 dB during the whole working band.

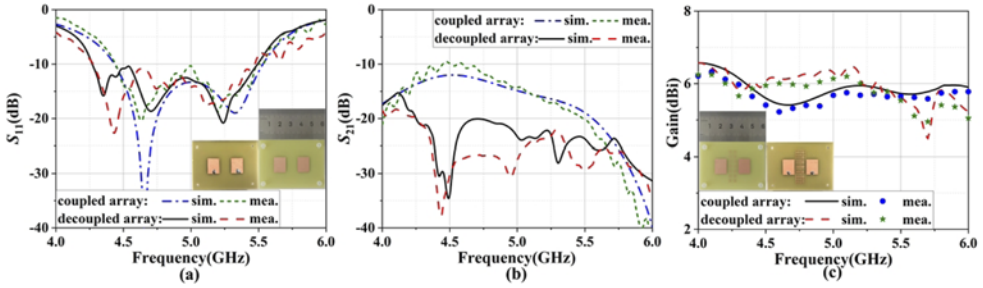

Fig. 5. Simulated and measured *S*-parameters, gains of two-element H-plane coupled and decoupled arrays, and their fabricated porotypes. (a) S_{11} and fabricated coupled antenna array; (b) S_{21}; (c) gain and fabricated decoupled antenna array.

The resulting gains of arrays when port 1 is excited and port 2 is terminated to a matching load are plotted in Fig. 5(c). In comparison to that of the single antenna in Fig. 3(d), the gain loss of the coupled array is 1.87 dB on average. The loaded metasurface partially aids the array element in improving the gain at most frequencies, and the average loss is 1.38 dB, though which is still large on account of the coupling that cannot be absolutely eliminated, the values are better than those of the coupled array. Moreover, the simulated and measured normalized radiation patterns of coupled and decoupled arrays at two typical frequencies (4.6 and 5.4 GHz) are displayed in Fig. 6. Because the antenna arrays are arranged along the H-plane, the proposed metasurface virtually causes no change to the E-plane radiation patterns. For the coupled plane, the strong mutual coupling deteriorates the radiation patterns and causes the directions to deviate, particularly apparent at 4.6 GHz, corresponding to the large coupling coefficient. However, due to the metasurface, the radiation patterns of the decoupled array compared with those of the coupled array become relatively normal.

To directly exhibit the decoupling effect, the current distributions of these two arrays at 4.6 GHz and 5.4 GHz are demonstrated in Fig. 7. Before decoupling, the energy coupled from port 1 to port 2 is extremely strong, and intensely concentrated current is distributed on the right antenna. However, the loaded metasurface efficiently impedes energy transmission, considerably alleviating coupling, as reflected by the weaker current distribution. The weak current distributions account for the decoupling principle of the proposed metasurface. In Fig. 7(b), the lower part of the metasurface distinctly performs a dominant role in restraining current transmission to the right antenna at a low frequency, causing the *y*-component of the electrical field to travel along the *y*-axis and the electromagnetic wave to turn evanescent. Meanwhile, at a high frequency, the upper

Optics EXPRESS

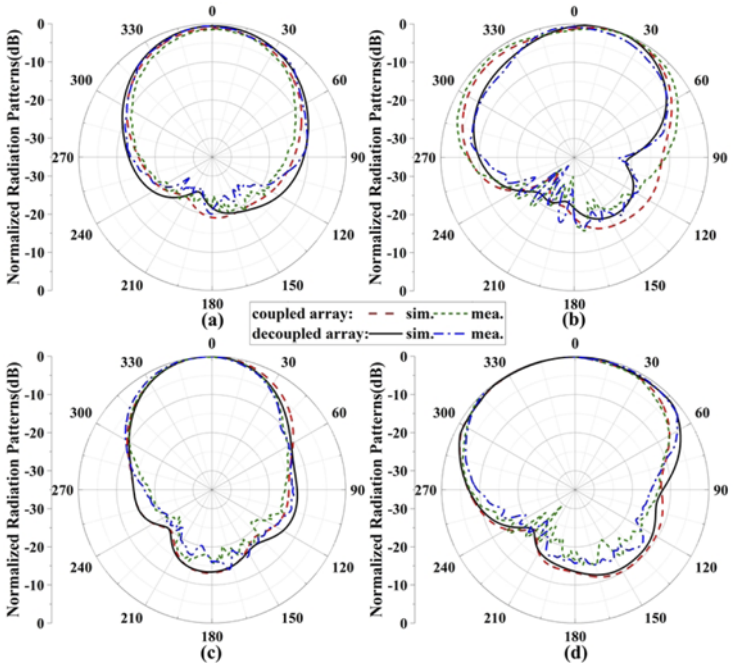

Fig. 6. Simulated and measured normalized radiation patterns of two-element H-plane coupled and decoupled arrays. (a) E-plane at 4.6 GHz; (b) H-plane at 4.6 GHz; (c) E-plane at 5.4 GHz; (d) H-plane at 5.4 GHz.

and lower parts both work to reverse the electrical field, deriving weak coupling compared with that of the original coupled array. Thus, the results indicate the superior decoupling capability of the proposed metasurface for a wideband two-element H-plane MIMO antenna array.

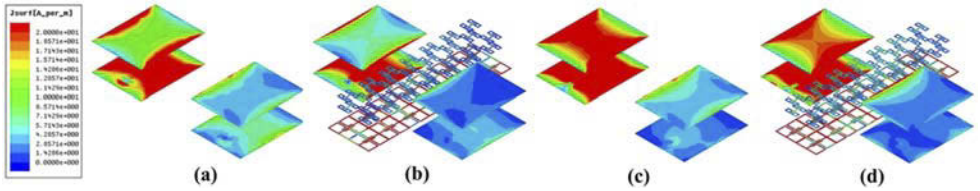

Fig. 7. Current distributions of two-element H-plane coupled and decoupled arrays. (a) Coupled array at 4.6 GHz; (b) decoupled array at 4.6 GHz; (c) coupled array at 5.4 GHz; (d) decoupled array at 5.4 GHz.

For a multielement MIMO antenna array, non-adjacent coupling must also be considered. Accordingly, a three-element H-plane coupled antenna array, presented in Fig. 8(a), is constructed to demonstrate the decoupling effectiveness of the proposed metasurface. Because the array is symmetric along the median, only the left middle antennas (Ant. 1 and Ant. 2) are thoroughly studied. Based on Fig. 8(b), which plots the related *S*-parameters, the added metasurface apparently enables the shared operating band to extend from 4.52-5.52 GHz (20.0%) to 4.36-5.52 GHz (23.5%). In contrast, both adjacent (S_{21}) and non-adjacent (S_{31}) mutual couplings are less than −20 dB. Moreover, the gains of Ant. 1 and Ant. 2 partially improve a bit. Consequently, the proposed metasurface remains to have ascendant capability in decoupling the multi-element MIMO antenna array.

Optics EXPRESS

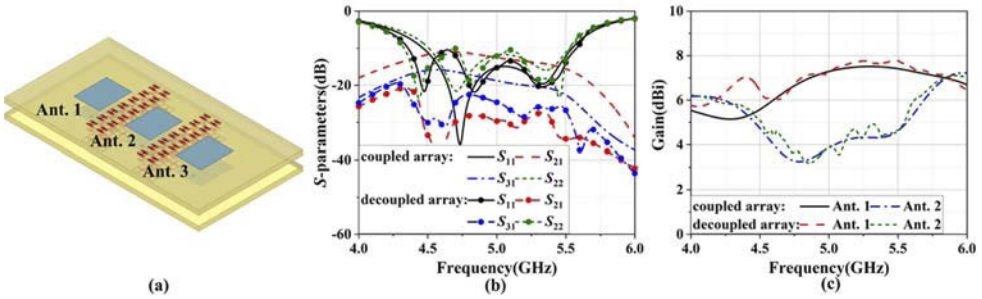

Fig. 8. Geometry and characteristics of three-element H-plane decoupled array compared with coupled array. (a) Three-element MIMO antenna array with metasurface; (b) *S*-parameters; (c) gains.

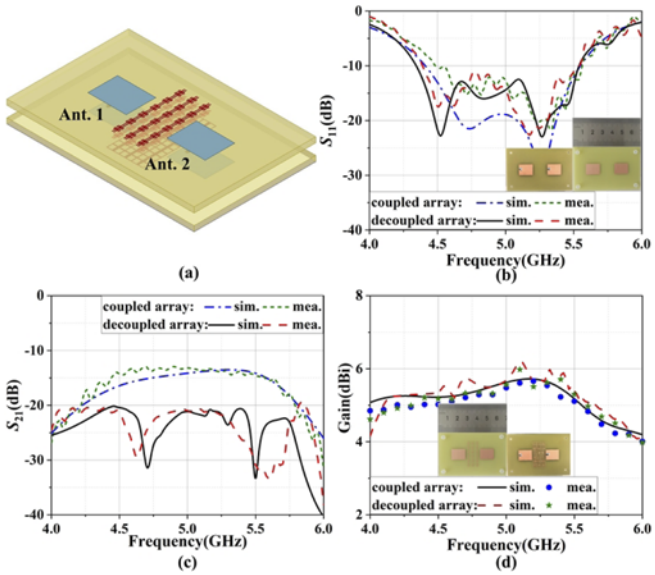

Fig. 9. Geometry of two-element E-plane decoupled array as well as its simulated and measured characteristics compared with the coupled array. (a) Two-element E-plane MIMO antenna array with metasurface; (b) S_{11} and fabricated coupled antenna array; (c) S_{21}; (d) gain and fabricated decoupled antenna array.

Then, to unlock the restraint of the array arrangement direction, the proposed metasurface (in a 6 × 3 sequence) is employed in a two-element E-plane coupled MIMO antenna array, as displayed in Fig. 9(a). To achieve satisfactory decoupling performance, the meta-atom dimensions are optimized. The edge-to-edge spacing of array elements is $d = 15$ mm ($0.25\lambda_0$); hence, the center-to-center spacing is $0.49\lambda_0$. Based on the *S*-parameters exhibited in Fig. 9(b) and (c), the measured operating band is found to slightly widen from 4.5-5.56 GHz (21.1%) to 4.4-5.54 GHz (22.9%). The mutual coupling coefficients are all less than −20 dB with the maximum and average reductions reaching 17.0 (at 5.52 GHz) and 9.6 dB, respectively. The gain of the decoupled array mostly slightly exceeds that of the coupled array. The current distributions of the coupled and decoupled arrays shown in Fig. 10 indicate that the coupling currents are greatly reduced, and virtually no current is transmitted to the right antenna. All of the above

Optics EXPRESS

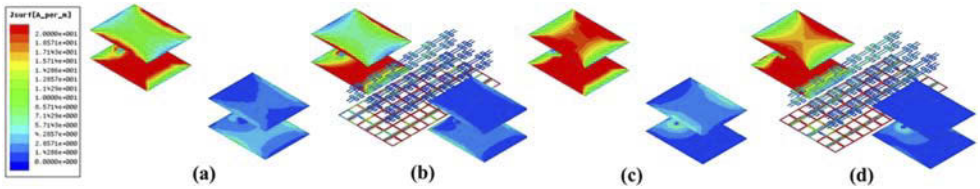

Fig. 10. Current distributions of two-element E-plane coupled and decoupled arrays. (a) Coupled array at 4.6 GHz; (b) decoupled array at 4.6 GHz; (c) coupled array at 5.4 GHz; (d) decoupled array at 5.4 GHz.

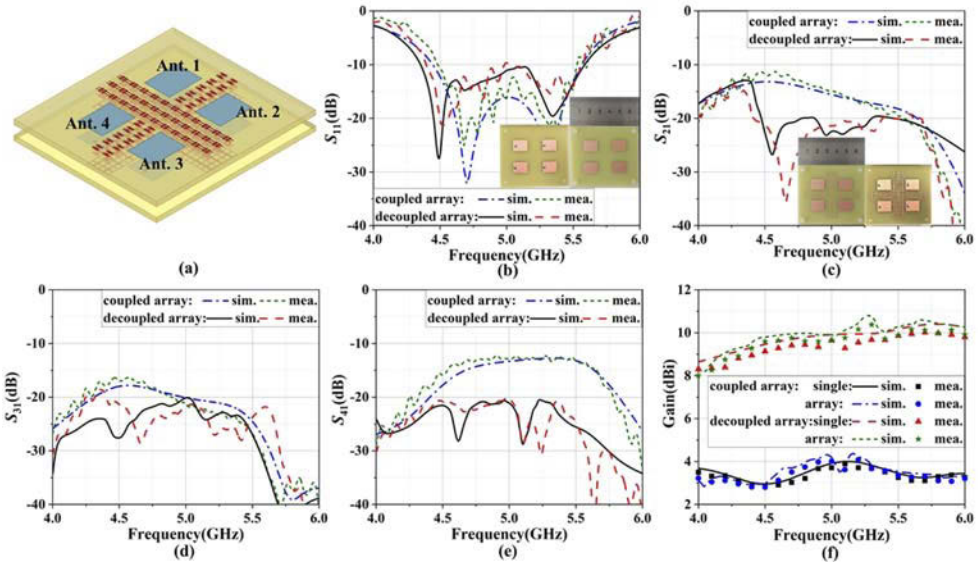

Fig. 11. Geometry of simulated and fabricated two-dimensional four-element MIMO antenna arrays as well as their simulated and measured characteristics compared with the coupled array. (a) Two-dimensional four-element MIMO antenna array with metasurface; (b) S_{11} and fabricated coupled antenna array; (c) S_{21} and fabricated decoupled antenna array; (d) S_{31}; (e) S_{41}; (f) gains of single Ant. 1 and entire array.

results ensure that the proposed metasurface has excellent capability in decoupling the wideband two-element E-plane MIMO antenna array, indicating its potential use in two-dimensional arrays.

Finally, having successfully verified the proposed metasurface in decoupling both H-plane and E-plane wideband MIMO antenna arrays, its decoupling performance in two-dimensional arrays is further evaluated. The geometry of a two-dimensional four-element MIMO decoupled antenna array equipped with the proposed metasurface and its characteristics are compared with those of the coupled array, as presented in Fig. 11. The antenna elements are arranged clockwise with element distances in two dimensions left unchanged. The metasurface utilizes the elements in the two-element E-plane array as the main part, whereas those in the H-plane array are extended on both sides. Then, the coupled and decoupled two-dimensional antenna arrays are simulated, fabricated, and measured; the *S*-parameters and gains are plotted in Fig. 11. The loaded metasurface definitely extends the measured operating bandwidth from 20.4% (4.5-5.52 GHz) to 23.6% (4.4-5.58 GHz). Based on all coupling coefficients related to Ant. 1 (i.e., S_{21}, S_{31}, and S_{41} shown in Fig. 10(c), (d), and (e), respectively), the metasurface can be adjudged capable of efficiently reducing mutual coupling. Compared with the coupling in the coupled array,

Optics EXPRESS

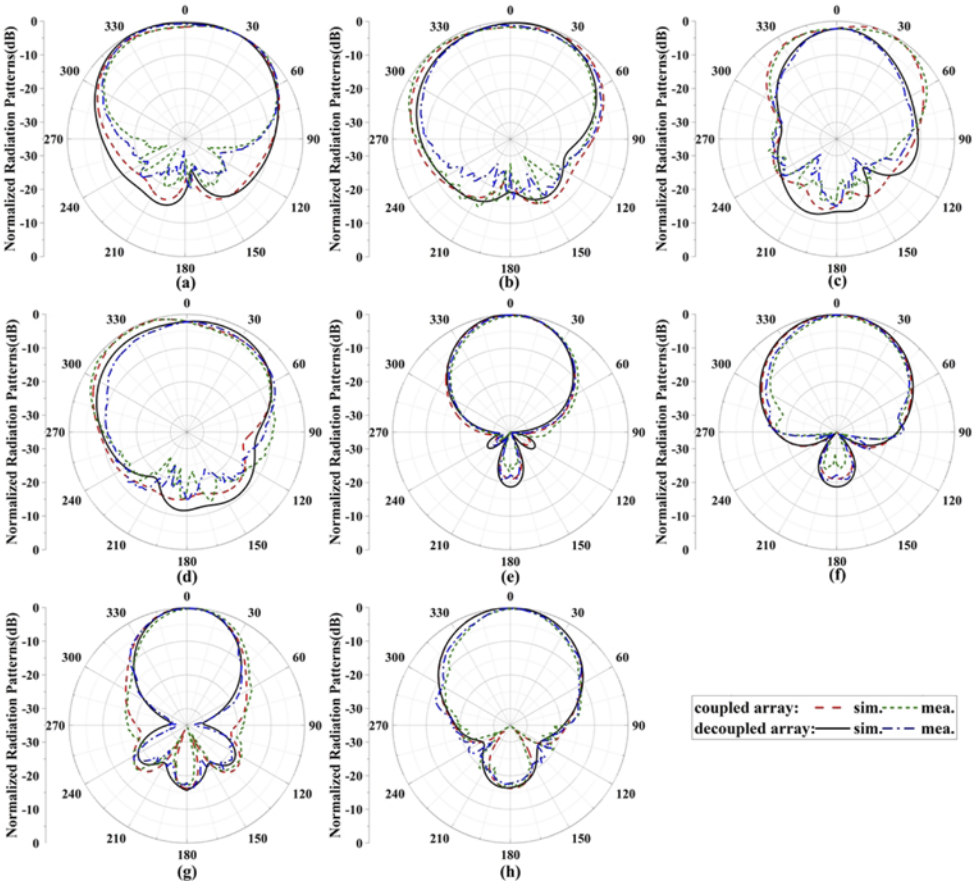

Fig. 12. Simulated and measured normalized radiation patterns of two-dimensional four-element coupled and decoupled arrays. (a) E-plane of single element at 4.6 GHz; (b) H-plane of single element at 4.6 GHz; (c) E-plane of single element at 5.4 GHz; (d) H-plane of single element at 5.4 GHz; (e) E-plane of entire array at 4.6 GHz; (f) H-plane of entire array at 4.6 GHz; (g) E-plane of entire array at 5.4 GHz; (h) H-plane of entire array at 5.4 GHz.

Table 2. Comparison of reported metasurface-based decoupling results.

Reference	Array arrangement	Array profile	Decoupling bandwidth
20	H-plane	$0.18\lambda_0$	8.5% (−20 dB)
21	H-plane	$0.20\lambda_0$	1.1% (−20 dB)
	E-plane	$0.21\lambda_0$	1.4% (−20 dB)
22	H-plane	$0.17\lambda_0$	22.3% (−15 dB)
23	H-plane	$0.44\lambda_0$	11.4% (−20 dB)
	E-plane	$0.38\lambda_0$	
24	H-plane	$0.16\lambda_l$/$0.21\lambda_h$	7.7%/5.7% (−20 dB)
25	H-plane	$0.15\lambda_0$	7.3% (−20 dB)
26	H-plane	$0.52\lambda_0$	6.1% (−20 dB)
This work	H-plane	$0.13\lambda_0$	25.4% (−20 dB)
	E-plane		22.9% (−20 dB)
	Two-dimension		23.6% (−20 dB)

Optics EXPRESS

especially at low band, that in the working band is less than −20 dB, which is a considerable improvement. Moreover, as shown in Fig. 11(f), the gains of single Ant. 1 of the decoupled array compared with those of the coupled array demonstrate that the metasurface is advantageous to gain improvement at most frequencies. While regarding to the entire arrays with all ports excited, the gains of the decoupled array are larger than those of the coupled one in the whole operating band. The simulated and measured normalized radiation patterns of the coupled and decoupled arrays including those of single element Ant. 1 and the entire array at 4.6 and 5.4 GHz are plotted in Fig. 12. As shown in Fig. 12(a)-(d), the E-plane and H-plane radiation patterns of the single element deviate from the broadside but shift to the normal direction after the proposed metasurface is loaded. According to Fig. 12(e)-(h), the shapes of the entire array's radiation patterns are satisfactory. Accordingly, the proposed metasurface is verified to be efficient in decoupling a two-dimensional MIMO antenna array.

To further demonstrate the superiority of the proposed decoupling metasurface, its performance is compared with the reported metasurface-based decoupling results in array profile and decoupling bandwidth, as listed in Table 2. Because the metasurface is coplanar with the arrays, it is noteworthy that the MIMO antenna arrays loaded with the proposed metasurface have the lowest array profile; this differs from all other works in which metasurfaces are placed above the arrays. Moreover, the decoupling bandwidths of these decoupled arrays are wider than those in other works. Thus, the proposed metasurface evidently exhibits better decoupling performance in the array profile and decoupling bandwidth.

4. Conclusions

In this paper, a novel metasurface is proposed to decouple wideband MIMO antenna arrays. The decoupling mechanism is based on network and field theories and implemented via the multilayer hybrid SRR meta-atom with single negative characteristic. The proposed metasurface is applied to decouple two-element H-plane, three-element H-plane, two-element E-plane wideband dual-layer coupled microstrip patch antenna arrays as well as a two-dimensional array. The decoupling results indicate that the working bandwidths of all decoupled arrays exceed 22%, mutual coupling is suppressed to less than −20 dB, gains mostly improve, and radiation patterns are modified. Additionally, different from reported metasurface-based decoupling works in which array profiles typically increase due to the metasurface placement above the arrays, the proposed metasurface does not modify the profiles. With these results, the proposed metasurface is anticipated to have a promising application to multielement large-scale wideband MIMO antenna arrays.

Funding. Natural Science Foundation of Shaanxi Province (2020JQ-482); National Natural Science Foundation of China (61871394).

Disclosures. The authors declare no conflicts of interest.

Data availability. Data underlying the results presented in this paper are not publicly available at this time but may be obtained from the authors upon reasonable request.

References

1. N. F. Yu, P. Genevet, M. A. Kats, F. Aieta, J. P. Tetienne, F. Capasso, and Z. Gaburro, "Light propagation with phase discontinuities: generalized laws of reflection and refraction," Science **334**(6054), 333–337 (2011).
2. L. X. Liu, X. Q. Zhang, M. Kenney, X. Q. Su, N. N. Xu, C. M. Ouyang, Y. L. Shi, J. G. Han, W. L. Zhang, and S. Zhang, "Broadband metasurfaces with simultaneous control of phase and amplitude," Adv. Mater. **26**(29), 5031–5036 (2014).
3. X. Li, S. Y. Xiao, B. G. Cai, Q. He, T. J. Cui, and L. Zhou, "Flat metasurfaces to focus electromagnetic waves in reflection geometry," Opt. Lett. **37**(23), 4940–4942 (2012).
4. W. K. Pan, T. Cai, S. W. Tang, L. Zhou, and J. F. Dong, "Trifunctional metasurfaces: concept and characterizations," Opt. Express **26**(13), 17447–17457 (2018).
5. Y. Z. Ran, J. G. Liang, T. Cai, W. Y. Ji, and G. M. Wang, "High-performance broadband vortex beam generator based on double-layered reflective metasurface," AIP Adv. **8**(9), 095201 (2018).
6. B. C. Pan and T. J. Cui, "Broadband decoupling network for dual-band microstrip patch antennas," IEEE Trans. Antennas Propag. **65**(10), 5595–5598 (2017).

Optics EXPRESS

7. S. Sui, H. Ma, Y. G. Lv, J. F. Wang, Z. Q. Li, J. Q. Zhang, Z. Xu, and S. B. Qu, "Fast optimization method of designing a wideband metasurface without using the Pancharatnam-Berry phase," Opt. Express **26**(2), 1443–1451 (2018).
8. H. P. Li, G. M. Wang, J. G. Liang, X. J. Gao, H. S. Hou, and X. Y. Jia, "Single-layer focusing gradient metasurface for ultrathin planar lens antenna application," IEEE Trans. Antennas Propag. **65**(3), 1452–1457 (2017).
9. N. S. Nie, X. S. Yang, Z. N. Chen, and B. Z. Wang, "A low-profile wideband hybrid metasurface antenna array for 5G and WiFi systems," IEEE Trans. Antennas Propag. **68**(2), 665–671 (2020).
10. T. Li and Z. N. Chen, "A dual-band metasurface antenna using characteristic mode analysis," IEEE Trans. Antennas Propag. **66**(10), 5620–5624 (2018).
11. D. X. Chen, W. C. Yang, Q. Xue, and W. Q. Che, "Miniaturized wideband planar antenna using interembedded metasurface structure," IEEE Trans. Antennas Propag. **69**(5), 3021–3026 (2021).
12. H. Q. Ngo, E. G. Larsson, and T. L. Marzetta, "Energy and spectral efficiency of very large multiuser MIMO systems," IEEE Trans. Commun. **61**(4), 1436–1449 (2013).
13. M. M. Bait-Suwailam, M. S. Boybay, and O. M. Ramahi, "Electromagnetic coupling reduction in high-profile monopole antennas using single-negative magnetic metamaterials for MIMO applications," IEEE Trans. Antennas Propag. **58**(9), 2894–2902 (2010).
14. H. X. Xu, G. M. Wang, M. Q. Qi, and H. Y. Zeng, "Ultra-small single-negative electric metamaterials for electromagnetic coupling reduction of microstrip antenna array," Opt. Express **20**(20), 21968–21976 (2012).
15. X. M. Yang, X. G. Liu, X. Y. Zhou, and T. J. Cui, "Reduction of mutual coupling between closely packed patch antennas using waveguided metamaterials," IEEE Antennas Propag. Lett. **11**, 389–391 (2012).
16. M. C. Tang, Z. Y. Chen, H. Wang, M. Li, B. Luo, J. D. Wang, Z. L. Shi, and R. W. Ziolkowski, "Mutual coupling reduction using meta-structures for wideband, dual-polarized, and high-density patch arrays," IEEE Trans. Antennas Propag. **65**(8), 3986–3998 (2017).
17. A. Jafargholi, A. Jafargholi, and J. H. Choi, "Mutual coupling reduction in an array of patch antennas using CLL metamaterial superstrate for MIMO applications," IEEE Trans. Antennas Propag. **67**(1), 179–189 (2019).
18. F. M. Yang, L. Peng, X. Liao, K. S. Mo, X. Jiang, and S. M. Li, "Coupling reduction for a wideband circularly polarized conformal array antenna with a single-negative structure," IEEE Antennas Propag. Lett. **18**(5), 991–995 (2019).
19. F. Khajeh-Khalili, M. A. Honarvar, M. Naser-Moghadasi, and M. Dolatshahi, "High-gain, high-isolation, and wideband millimetre-wave closely spaced multiple-input multiple-output antenna with metamaterial wall and metamaterial superstrate for 5G applications," IET Microw. Antennas Propag. **15**(4), 379–388 (2021).
20. Z. Y. Wang, L. Y. Zhao, Y. M. Cai, S. F. Zheng, and Y. Z. Yin, "A meta-surface antenna array decoupling (MAAD) method for mutual coupling reduction in a MIMO antenna system," Sci. Rep. **8**(1), 3152 (2018).
21. H. Z. Luan, C. Chen, W. D. Chen, L. Y. Zhou, H. L. Zhang, and Z. X. Zhang, "Mutual coupling reduction of closely E/H-plane coupled antennas through metasurfaces," IEEE Antennas Propag. Lett. **18**(10), 1996–2000 (2019).
22. L. M. Si, H. X. Jiang, X. Lv, and J. Ding, "Broadband extremely close-spaced 5G MIMO antenna with mutual coupling reduction using metamaterial-inspired superstrate," Opt. Express **27**(3), 3472–3482 (2019).
23. J. Y. Guo, F. Liu, L. Y. Zhao, Y. Z. Yin, G. L. Huang, and Y. S. Li, "Meta-surface antenna array decoupling designs for two linear polarized antennas coupled in H-plane and E-plane," IEEE Access **7**, 100442–100452 (2019).
24. F. Liu, J. Y. Guo, L. Y. Zhao, G. L. Huang, Y. S. Li, and Y. Z. Yin, "Dual-band metasurface-based decoupling method for two closely packed dual-band antennas," IEEE Trans. Antennas Propag. **68**(1), 552–557 (2020).
25. Z. Y. Wang, C. L. Li, and Y. Z. Yin, "A meta-surface antenna array decoupling (MAAD) design to improve the isolation performance in a MIMO system," IEEE Access **8**, 61797–61805 (2020).
26. Z. Xu, Z. Zhao, Q. S. Zhang, S. C. Yan, L. Y. Guo, Z. W. Yang, M. J. Guo, and Z. Y. Wang, "Mutual coupling reduction in planar Yagi antenna array using bidirectional absorbing metasurface," Int. J. RF Microw. Comput. Aided Eng. **30**(2), e22051 (2020).
27. X. D. Chen, T. M. Grzegorczyk, B. I. Wu, J. Pacheco, and J. A. Kong, "Robust method to retrieve the constitutive effective parameters of metamaterials," Phys. Rev. E **70**(1), 016608 (2004).